



ISTITUTO NAZIONALE DI RICERCA METROLOGICA Repository Istituzionale

Rapid and sensitive detection of pyrimethanil residues on pome fruits by Surface Enhanced Raman Scattering

This is the author's submitted version of the contribution published as:

Original

Rapid and sensitive detection of pyrimethanil residues on pome fruits by Surface Enhanced Raman Scattering / Mandrile, L; Giovannozzi, A M; Durbiano, F; Martra, G; Rossi, A M. - In: FOOD CHEMISTRY. - ISSN 0308-8146. - 244:(2018), pp. 16-24-24. [10.1016/j.foodchem.2017.10.003]

Availability:

This version is available at: 11696/57293 since: 2021-03-09T19:21:03Z

Publisher:

Elsevier

Published

DOI:10.1016/j.foodchem.2017.10.003

Terms of use:

This article is made available under terms and conditions as specified in the corresponding bibliographic description in the repository

Publisher copyright

(Article begins on next page)

Elsevier Editorial System(tm) for Food

Chemistry

Manuscript Draft

Manuscript Number: FOODCHEM-D-17-01263R1

Title: Rapid and sensitive detection of pyrimethanil residues on pome fruits by surface enhanced Raman scattering

Article Type: Analytical Methods Article

Keywords: pyrimethanil, pome fruits, Surface Enhanced Raman Scattering, Raman Spectroscopy, gold nanoparticles, Partial Least Squares

Corresponding Author: Dr. Andrea Mario Giovannozzi, Ph.D.

Corresponding Author's Institution: INRIM

First Author: Luisa Mandrile

Order of Authors: Luisa Mandrile; Andrea M Giovannozzi, Phd; Francesca Durbiano, Phd; Gianmario Martra, Professor; Andrea M Rossi, Phd

1 *This manuscript represents an updated and extended version of the paper*
2 *“Surface Enhanced Raman Spectroscopy: A Metrological Tool for Fungicide Detection”*
3 *Presented at the 2nd IMEKOFODS Conference “Metrology Promoting*
4 *Objective and Measurable Food Quality & Safety” (Benevento, Italy – 2nd - 5th*
5 *October 2016), selected for publication in Food Chemistry*

6 **Rapid and sensitive detection of**
7 **pyrimethanil residues on pome fruits by**
8 **surface enhanced Raman scattering**

9 L. Mandrile^{a,b}, A. M. Giovannozzi^{a,*}, F. Durbiano^a, G. Martra^b and

10 A. M. Rossi^a

11 ^a *Division of Metrology for Quality of Life, Istituto Nazionale di Ricerca Metrologica, Strada*
12 *delle Cacce, 91 10135, Torino, Italy*

13 ^b *Department of Chemistry and Interdepartmental Centre NIS, University of Turin, Via Giuria*
14 *7, 10125, Turin, Italy*

15 ^{*} *Corresponding author: Andrea M. Giovannozzi, tel +39 011 3919330; fax +39 011 346384;*
16 *e-mail a.giovannozzi@inrim.it*

17

18 **Abstract**

19 Surface Enhanced Raman Scattering (SERS) supported by gold nanoparticles (AuNPs) was
20 applied to detect and quantify residues of pyrimethanil on pome fruits, a widely used
21 fungicide in horticultural species. Spheroidal AuNPs with different size were fabricated and
22 compared in this study. The analytical procedure was set up on a silicon dioxide flat substrate
23 to standardize SERS methodology. A Raman mapping strategy was exploited to increase
24 signal reproducibility and to minimize bias due to different local surface morphologies.
25 Univariate and multivariate regressions were compared for calibration. **Multivariate PLS**
26 **approach demonstrated acceptable repeatability and method stability (RMSECV = 4.79 ppm;**
27 **RMSEP= 4.31ppm) in the range 0 - 40 mg kg⁻¹, providing higher accuracy and intra-day**
28 **repeatability with a mean percentage error of 18.7 % and 32.8 % for PLS and univariate**
29 **calibration, respectively. The method here proposed can be reliably applied for PMT detection**
30 **on pome fruits within the European law limits.**

31

32

33

34 *keywords: pyrimethanil, pome fruits, Surface Enhanced Raman Scattering, Raman*
35 *spectroscopy, gold nanoparticles, Partial Least Squares*

36

37 1. Introduction

38 In the last decades food safety incidents have raised public concern about synthetic additives
39 and chemical contaminants in food, the latter of them are mainly agricultural and
40 environmental, chemical adulterants, mycotoxins, and foreign food components (Zheng J, He
41 L, 2014). Agrochemical products such as pesticides and fungicides are normally applied to
42 protect food crops from the pests at various stages of cultivation and during post-harvest
43 storage (Sharma RR, Singh D, Singh R, 2009), but their intensive use can generate residues
44 that may become a potential risk for both public health and environment (Gilden RC, Huffling
45 K, Sattler B, 2010). Pyrimethanil [(PMT), N-(4,6-dimethylpyrimidin-2-yl)-phenylamine] is a
46 fungicide belonging to the anilinopyrimidine class of pesticides which inhibits the secretion of
47 hydrolytic enzymes by the fungi during the infection process, thus stopping penetration and
48 development of the disease [FAO, 2007]. This broad spectrum fungicide is effectively used
49 for the control of gray mould, leaf scab and other postharvest diseases on pome fruits,
50 vegetables and ornamentals (Yu C, Zhou T, Sheng K, Zeng L, Ye C, Yu T, Zheng X, 2013).
51 Even if PMT demonstrated low acute toxicity in mammals, long-term studies showed certain
52 toxicity in mice, rats, dogs and aquatic organisms with potential carcinogenicity. Owing to its
53 toxicity and wide application on horticultural species, PMT has been included as a pesticide
54 by the Commission Directive 2006/74/EC of August 2006 with a maximum residue level of 7
55 mg kg⁻¹ on pome fruits (Regulation (EC) No 396/2005). Most of the published methods for
56 the determination of PMT on fruits, vegetables and other samples are usually based on GC
57 (Amvrazi EG, Tsiropoulos NG, 2009) , GC-MS/MS (Raeppl C, Nief M, Fabritius M,
58 Racault L, Appenzeller BM, Millet M, 2011; Rodriguez-Cabo T, Rodriguez I, Ramil M, Cela
59 R, 2011), GC-MS ([Gonzalez-Rodriguez RM, Rial-Otero R, Cancho-Grande B, Simal-
60 Gandara J, 2008) LC-MS (Park S et al 2010), HPLC (Zhou Y et al 2011), and LC-MS/MS

61 (Ortelli D, Edder P, Corvi C, 2004). These methods have high accuracy, good reproducibility
62 and provide quantitative determination of PMT according to the EU limits, but they also
63 suffer from inevitable disadvantages such as expensive experimental instruments, trained
64 personnel and time-consuming extraction steps. Therefore, the development of more rapid
65 and user friendly methods for PMT residues detection on horticultural species is highly
66 required.

67 New methodologies based on ELISA (Mercader JV, Esteve-Turrillas FA, Agullo C, Abad-
68 Somovilla A, Abad-Fuentes A, 2012) and electrochemical sensors (Garrido JMPJ, Rahemi V,
69 Borges F, Brett CMA, Garrido EMPJ, 2016; Yang J, Wang Q, Zhang M, Zhang S, Zhang L,
70 2015) were recently proposed as interesting alternatives to the traditional analytical methods,
71 providing high selectivity and sensitivity in PMT detection in real samples. However, no
72 studies were made so far concerning the development of a PMT detection tool based on
73 Surface Enhanced Raman Scattering (SERS). Compared with the conventional analytical
74 techniques, Raman spectroscopy allows fast detection times, high selectivity due to the
75 Raman fingerprint of molecules and minimal or no preliminary treatment of the sample.
76 Moreover, the sensitivity of the normal Raman technique can be increased by several orders
77 of magnitude in SERS analysis due to the enhancement of the Raman scattering of molecules
78 absorbed onto, or microscopically close to, a suitable plasmonically active surface, such as
79 roughened nanostructured metal surface, or metal colloids (Schluecker S, 2014). For all these
80 reasons SERS represents a good candidate in food control analysis. Different SERS
81 approaches were already reported on the detection of various classes of pesticides in real-food
82 matrices. In case of solid matrices, homogenization of the peel or surface swab methods were
83 used to recover pesticides from the surface and the detection was subsequently performed
84 using solid surface-based substrates (He L, Chen T, Labuza TP, 2014; Fan Y, Lai K, Rasco

85 BA, Huang Y, 2014). *In situ* detection of pesticides in fruits was also demonstrated using
86 different types of metal nanoparticles (NPs) (Li FJ et al 2010; Liu B et al 2012) which were
87 spread as “smart dust” over the surface that has to be probed. However, even if these SERS
88 substrates demonstrated to achieve a very high sensitivity in the detection of chemical
89 contaminants, they usually suffer from lack of reproducibility and inconsistent performance
90 when spot-to-spot tests are conducted, leading to problems in the quantification process.
91 Therefore, standardized SERS tool with a good compromise between sensitivity and
92 reproducibility of analysis are needed to provide reliable analytical methods in the detection
93 of food contaminants.

94 In this work we propose a versatile, simple and reproducible procedure to detect, discriminate
95 and quantify residues of pyrimethanil on pome fruits by SERS. We selectively tested
96 spheroidal AuNPs with different dimensions in order to have the highest SERS effect. The
97 analytical procedure was set up on a flat surface as model system to standardize SERS
98 methodology for both qualitative and quantitative analysis. Raman mapping was exploited to
99 increase signal reproducibility from spot to spot analysis and to provide more consistent
100 results. A semi-quantitative *in situ* detection method on fruit peel was assessed and an
101 accurate method for pyrimethanil quantification on fruit surface was developed and validated.

102

103

104 **2. Material and Methods**

105 *2.1 Reagents and materials*

106 Hydrogen tetrachloroaurate trihydrate ($\text{HAuCl}_4 \cdot 3\text{H}_2\text{O} \geq 99\%$), trisodium citrate dihydrate
107 ($\geq 99\%$), were purchased from Sigma-Aldrich (Milan, Italy). Sodium hydroxyde (NaOH

108 97%), Hydrochloric acid (HCl 37%), Nitric acid (HNO₃ 68%), absolute ethanol (99.99%),
109 acetone (99,99%) and Hydroxylamine Hydrochloride (H₃NO·HCl, 99+%) were obtained by
110 Novachimica (Milano, Italy). Scala® (400 g/l of Pyrimethanil suspension) was purchased
111 from BASF Italia (Volpiano, Italy). All solutions were prepared with Milli-Q quality water
112 (18 MΩcm). Silicon wafers with a 300 nm of Silicon dioxide layer on top were purchased
113 from Si-Mat (Kaufering, Germany). Apples used for the assays were purchased in a local
114 supermarket in Torino, Italy.

115

116 *2.2 Gold nanoparticles preparation*

117 All glassware used in the experiment was soaked in aqua regia (HCl:HNO₃ 3:1 v/v) and
118 rinsed thoroughly in water and dried with nitrogen prior to use. Spheroidal AuNPs with a
119 diameter of about 30 nm, 40 nm and 55 nm were synthesized according to Frens G, 1973.
120 Briefly, 7 ml, 5 ml and 3.5 ml of a 1% aqueous solution of trisodium citrate were rapidly
121 injected into 500 ml boiling solution of HAuCl₄ (0.01% v/v) for the preparation of 30 nm, 40
122 nm and 55 nm AuNPs, respectively. The mixture was further refluxed for 10 min and then
123 cooled to room temperature under continuous stirring. Larger AuNPs with a diameter of 90
124 nm and 120 nm were obtained via seed-mediated growth of 30 nm and 40 nm AuNPs,
125 respectively, using an optimized growing procedure based on hydroxylamine hydrochloride
126 (Li JF, 2013). In detail, 4 ml of Au seeds suspension were put into a round-bottom flask with
127 53.8 ml of Milli-Q water under continuous stirring and the different solutions were added in
128 the following order: 920 µl of 1% v/v aqueous solution of trisodium citrate (stirring for 3
129 min), 1.4 ml of 10 mM hydroxylamine hydrochloride solution (stirring for 8 min) and 90 µl of
130 10% w/v HAuCl₄ (added dropwise, 1 drop per second). The concentration of 30 nm, 55 nm,

131 90 nm and 120 nm AuNPs suspensions is $9 \cdot 10^{-11} \text{ mol l}^{-1}$, $6 \cdot 10^{-11} \text{ mol l}^{-1}$, $8 \cdot 10^{-12} \text{ mol l}^{-1}$, $6 \cdot 10^{-12} \text{ mol l}^{-1}$ respectively. The suspensions were kept in continuous stirring overnight at room
132 temperature in the dark before using it.
133

134 *2.3 Gold Nanoparticles Characterization*

135 AuNPs characterization was done by UV-Vis absorption measurements and by Scanning
136 Electron Microscopy (SEM) imaging. UV-Vis absorption spectra were collected in the
137 rang400-1100 nm with the Evolution 60s spectrophotometer (Thermo Scientific). The
138 wavelength resolution is 1 nm. SEM characterization was carried out using a SEM FEI
139 Inspect F in UHV mode with the secondary electrons (SE) detector. Typical settings for the
140 imaging are: 10 kV accelerating voltage, 2.5 electron beam spot (18 pA) or 3.5 spot (30pA),
141 10 mm WD. By imaging the particles using SEM, size and shape of AuNPs were
142 characterized as well as the size distribution of their particles. At least 300 nanoparticles were
143 counted for each sample to estimate the mean diameter and the relative standard deviation of
144 the AuNPs.

145

146 *2.4 Preparation of Pyrimethanil standard suspensions and solutions*

147 Pyrimethanil solubility in water at room temperature is 0,121 g/l; in case of higher
148 concentration it is dispersed in a stable suspension. Pyrimethanil stock standard suspension
149 was prepared by accurately diluting 2 ml of Scala® (400 g l^{-1} of Pyrimethanil suspension) in
150 100 ml and 200 ml of Milli-Q water, to reach a concentration of 8 g l^{-1} ($8 \cdot 10^3 \text{ ppm}$) and 4 g l^{-1} .
151 Pyrimethanil standard solutions were prepared by subsequent dilutions from the stock
152 suspensions in water to reach the following concentrations: 40 mg l^{-1} , 30 mg l^{-1} , 20 mg l^{-1} , 10

153 mg l⁻¹, 5 mg l⁻¹, 1 mg l⁻¹. These pure pyrimethanil standards were used for AuNPs aggregation
154 test, SERS efficiency test and to set up the analytical procedure.

155

156

157 *2.5 AuNPs aggregation test*

158 Aliquots of pyrimethanil standard suspension (400 mg l⁻¹) were mixed in a 1:2 ratio with
159 AuNPs stock suspension, mixed with vortex for 3 s and subsequently analyzed by UV-Vis. In
160 these conditions PMT is in high excess with respect to AuNPs and their interaction, if present
161 could not be negligible. Measurements in acidic conditions were performed after adding few
162 drops of 1 M HCl to reach a pH value close to 3. UV-Vis measurements were repeated over
163 four days.

164

165 *2.6 SERS Efficiency Test*

166 1 μl of a 400 mg l⁻¹ pyrimethanil standard suspension was deposited by drop casting on a flat
167 gold surface and let it dry in air for evaporation. 5 depositions were performed on the surface
168 in order to obtain an array of 5 pyrimethanil spots (4 spots for SERS collection and 1 spot for
169 normal Raman reference collection). Each spot was covered with 2 μl of AuNPs for Raman
170 mapping after drying. A reference spot for SERS analysis was also made by covering a PMT
171 spot with 2 μl of water. The concentration of all AuNPs suspension was levelled to have the
172 same exposed surface area (4×10^{12} nm²), avoiding bias in case of larger NPs.

173

174 *2.7 Detection of PMT on pome fruits*

175 Pome fruit samples such as green apples were bought from a local store. The whole fruit was
176 washed with sodium bicarbonate to remove contaminants from the surface and then spiked
177 with different amount of PMT standard suspensions. For the on-peel detection tests, the
178 spiking procedure was set using a manual nebulizer with 100 ml capacity in order to better
179 simulate the in-field pesticide diffusion on fruits. For the accurate contamination of the
180 sample to be used as validation test of the quantitative method, the PMT suspension was
181 deposited using a micro syringe with a 0.1 μ l precision.

182 *In situ* detection of pyrimethanil was performed by depositing 2 μ l of a 10-fold concentrated
183 120 nm AuNPs suspension on the contaminated peel, followed by Raman mapping after the
184 evaporation of the colloids suspension. The 10-fold concentrated 120 nm AuNPs suspension
185 was obtained by centrifugating the AuNPs stock suspension at 600 g for 12 min and
186 subsequently re-suspending in a proper amount of water suspension.

187 For an accurate and precise quantification of the fungicide on the entire surface of the fruit, an
188 extraction procedure was carried out by thoroughly rinsing the contaminated peel with a
189 known amount of distilled water (usually equal to the fruit weight) to recover pyrimethanil
190 from the surface. Three separated rinses using one third of the total washing volume were
191 performed to increase the extraction efficiency. 2 μ l of the resulting solution were deposited
192 by drop casting on a silicon dioxide surface and let them dry in air for evaporation. 2 μ l of a
193 10-fold concentrated 120 nm AuNPs suspension were then deposited on the PMT spot and
194 analyzed by Raman mapping after drying. The content of PMT in real samples was
195 determined by SERS according to the analytical procedure reported in 2.9.

196

197 *2.8 SERS Measurement*

198 SERS spectra were recorded using a Thermo Scientific DXR Raman equipped with a
199 microscope, excitation laser source at 780 nm, a motorized microscope stage sample holder,
200 and a charge-coupled device (CCD) detector. Raman equipment is monthly calibrated through
201 a software-controlled calibration tool which ensures wavelength calibration using multiple
202 neon emission lines, laser frequency calibration using multiple polystyrene Raman peaks,
203 intensity calibration using standardized white light sources. The frequency uncertainty is
204 determined by the grating resolution of 5 cm^{-1} (the grating groove density is 1200). The
205 intensity uncertainty was demonstrated to be lower than 5 % using a polystyrene standard.
206 Spectra of samples were collected using a 20x long working distance microscope objective
207 (spot size $1.7 \mu\text{m}$, N.A. 0.40) with a 10 mW laser power and a spectral range from 150 to
208 3400 cm^{-1} . The acquisition time for each spectrum was 1 second for 5 exposures. A Raman
209 map of about 25 spectra was collected on each PMT-AuNPs spot (about 0.5 mm^2 area was
210 investigated) and the obtained spectra were averaged for statistical analysis.

211 *2.9 Computational procedure*

212 Geometry optimization of model PMT structures and consequent calculations of vibrational
213 (IR and Raman) spectra were carried out with DFT method using Gaussian 03 program
214 (Gaussian 03, Revision B.05, References cited in <http://www.gaussian.com>). Full geometry
215 optimizations were carried out without symmetry constraints. The computations were
216 performed with the Lee, Yang and Parr correlation functional (LYP) (Lee C., Yang W, Parr
217 RG, 1998) combined with the Becke's non-local three-parameter hybrid exchange functional,
218 (B3) (Becke AD, 1993). Vibrational information coming from the computational procedure
219 were compared with the experimental Raman spectrum of PMT and the main bands in the
220 spectrum were assigned using the Handbook of Infrared and Raman Spectroscopy (Socrates G

221 “Infrared and Raman Characteristic Group Frequencies: Tables and Charts”, Wiley ISBN:
222 978-0-470-09307-8).

223

224 *2.10 Quantitative calibration and validation of the method*

225 The instrumental linearity was evaluated from a calibration curve calculated with five levels
226 of PMT concentrations in non-spiked fruit extract, representative of the analyzed matrix: 0 mg
227 kg^{-1} , 5 mg kg^{-1} , 10 mg kg^{-1} , 20 mg kg^{-1} , 40 mg kg^{-1} . 2 μl of each PMT standard solution were
228 deposited by drop casting on a silicon dioxide surface and let them dry in air for evaporation.
229 In the calibration procedure of SERS analysis, 2 μl of a 10-fold concentrated 120 nm AuNPs
230 suspension were deposited on the five spots with increasing concentrations of pyrimethanil.
231 After drying, Raman mapping was performed on each spot, as described in 2.8, and all spectra
232 from each map were averaged for statistical analysis. Each measurement was repeated 4 times
233 to test measurement repeatability for a total of 20 calibration standards. A specific AuNPs
234 Raman band at 2130 cm^{-1} was exploited to normalize the Raman intensity of pyrimethanil
235 spectrum, minimizing possible variations due to laser power, focal distance and
236 environmental parameters (temperature, humidity) and to overcome variations of the
237 enhancement effect due to the different ratio between the amount AuNPs and analyte
238 molecules. The uncertainty of pyrimethanil concentrations was also calculated, as
239 recommended by the GUM JCGM 100:2008 and Supplement 1 JCGM 101:2008, in order to
240 meet metrological requirements. The intensity of PMT Raman band at 997 cm^{-1} was plotted
241 versus pyrimethanil concentration to obtain the calibration curve. The applied fitting
242 procedure was a weighted total least square (WTLS) regression, and was implemented by
243 means of a MATLAB®-based tool for calibration problems that is able to deal with

244 uncertainty (and correlation) in both the dependent (average intensities) and independent
245 (mass values) variables; the Calibration Curve Computing Software for the evaluation of
246 instrument calibration curves is provided by the Italian national institute for metrological
247 research (INRiM). The linearity in the concentration range considered was estimated by the
248 reduced chi-square value (χ^2). Acceptability criterion to assume the linearity of response is a
249 χ^2 close to 1.

250 Multivariate calibration was performed using Partial Least Square method. PLS regression is
251 based on the maximization of the covariance between variables (spectral frequencies) and
252 response (contaminant concentration) associated to the calibration standards (Wold H, 2006).
253 Seven concentrations of pyrimethanil (0 mg kg⁻¹, 1 mg kg⁻¹, 5 mg kg⁻¹, 10 mg kg⁻¹, 16 mg kg⁻¹
254 20 mg kg⁻¹, 30 mg kg⁻¹, 40 mg kg⁻¹) were deposited and covered with AuNPs as described
255 above. For each standard 4 SERS maps were collected and the mean spectrum of each map
256 was used as calibration standard for a total of 32 calibration standards. PLS calculation was
257 performed using the PLS Toolbox for Matlab ®. PLS regression was applied to mean
258 centered SERS spectra. Spectral frequencies ranging from 180 cm⁻¹ to 2500 cm⁻¹ were
259 considered, excluding the first order of silicon in the range between 500 cm⁻¹ and 550 cm⁻¹
260 that was not included in the calibration process. The optimal number of PLS latent variables
261 was selected on the basis of the cumulative explained variance (CEV) for each component
262 and the root mean square error in cross validation (RMECV). The validation was performed
263 using a venetian blinds cross validation procedure with 6 cancellation segments at first for
264 method optimization and an external set of four samples for test set final validation.

265

266 **3. Results and Discussion**

267 Several studies already proposed metallic NPs as useful substrates for pesticides detection but
268 in most of these methods a strong chemical interaction between the colloids and the analyte
269 occurred. This binding affinity normally leads the aggregation of the NPs generating clustered
270 SERS hot spots which are responsible for a huge enhancement of their Raman signals. Unlike
271 it was previously reported, the chemical structure of pyrimethanil does not support selective
272 binding with citrate terminated AuNPs and the enhancement of its Raman signals can be
273 exclusively promoted by the electromagnetic effect, which has to be induced by the proximity
274 of the fungicide on the metallic NPs surface. The chemical interaction of AuNPs with
275 pyrimethanil was initially studied performing AuNPs aggregation test in suspension.
276 Spheroidal AuNPs with different size were fabricated, as reported in the paragraph 2.2, and
277 characterized by SEM and UV-Vis measurements. SEM images of AuNPs with the mean
278 diameter of 30 nm, 55 nm, 90 nm and 120 nm, respectively are shown in figure 1S in
279 supplementary information.

280 The UV-Vis absorption spectra of these NPs were acquired and they are reported in Figure 2S
281 in supplementary information. As the size of AuNPs increases, the λ_{\max} was found out to
282 increase from 530 nm to 580 nm, which agrees with the previous conclusion that the
283 maximum peak wavelength red-shifts as the relative particle size gets bigger (Hong S, Li X,
284 2013).

285 The chemical interaction of AuNPs with pyrimethanil was studied by means of a AuNPs
286 aggregation test (Figure 1), as reported in paragraph 2.5. A decreased stability of the colloids
287 in suspension would provoke the aggregation of AuNPs, inducing a shift of the localized
288 surface Plasmon resonance (LSPR) with a consequent variation of the colloidal system color
289 from red to blue, that can be easily monitored by UV-Vis absorption measurements.

290 The stability of the colloidal suspensions was monitored at acidic conditions (pH~3) in which
291 PMT is completely solubilized in water and its interaction with citrate-terminated AuNPs
292 should be maximized (pKa Pyrimethanil = 3.26). As Figure 1 shows, no shift of the LSPR
293 peaks at higher wavelengths was registered over 15 minutes for the 30 nm, 55 nm, 90 nm and
294 120 nm AuNPs colloids after adding PMT (400 mg l⁻¹), meaning that no, or very low,
295 chemical affinity exists between AuNPs and the analyte. No shift of the LSPR peaks was
296 further observed after four days, confirming the long term stability of all these colloidal
297 systems in the presence of PMT (Figure 1).

298 Fig. 1

299 Since PMT and AuNPs do not interact in a liquid medium, PMT detection has to be
300 conducted in dry condition in order to promote the absorption of the PMT on the AuNPs
301 surface and to maximize the electromagnetic effect in SERS technique.

302 A comparative SERS efficiency test using spheroidal AuNPs with a diameter of 30 nm, 55
303 nm, 90 nm and 120 nm was performed to investigate the effect of the nanoparticle size on the
304 Raman enhancement, as it was described in paragraph 2.6. The sum of surface area A of all
305 AuNPs was calculated using equation (1), assuming that all nanoparticles are spherical (Hong
306 S et al 2013)

$$A = 4\pi r^2 n = \frac{6\pi d^2 m_t}{D\pi d^3} = \frac{6m_t}{Dd} \quad (1)$$

307
308 where n is the number of nanoparticles; m_t is the total mass of Au in the suspension; D is the
309 density of Au assuming that the density does not change with the size of the nanoparticles; d
310 is the diameter of the nanoparticles.

311 To provide a consistent comparative study, the total surface area of AuNPs with different size
312 was kept the same in SERS efficiency test. The total surface area was normalized to the

313 surface area of a 10-fold concentrated 120 nm AuNPs suspension, corresponding to 4×10^{12}
314 nm^2 .

315 Normal Raman spectrum of PMT in solid state is shown in Figure 2. Typical Raman
316 fingerprint of pure PMT exhibits vibrational peaks at 560 cm^{-1} , 610 cm^{-1} , 620 cm^{-1} , 997
317 cm^{-1} , 1033 cm^{-1} , 1246 cm^{-1} and 1296 cm^{-1} whose assignments are reported in Figure 2. **Band**
318 **assignments for PMT molecule were obtained by a combination of a computational procedure**
319 **with vibrational information from Handbook of Infrared and Raman Spectroscopy, as**
320 **reported in the section 2.9 of Material and Methods.**

321 **Fig. 2**

322 As Figure 3 shows, SERS spectral features of PMT standard obtained with the all tested
323 AuNPs were consistent with its conventional Raman spectrum. The major characteristic peaks
324 found in the Raman spectrum of PMT (560 cm^{-1} , 610 cm^{-1} , 620 cm^{-1} , 997 cm^{-1} , 1033 cm^{-1})
325 were clearly visible in their SERS spectral counterparts. However, the relative intensities of
326 characteristic peaks may change, broadening of peaks may occur, and new peaks may show
327 up in the SERS spectra. For example, intensity of the characteristic double peak of PMT at
328 610 cm^{-1} , 620 cm^{-1} was increased, the peak at 560 cm^{-1} was broadened and a new peak at
329 950 cm^{-1} showed up in SERS spectra compared to its conventional Raman spectrum. These
330 changes were due to the interactions of analyte molecules with the surfaces of gold
331 nanoparticles, in particular related to the orientations of analyte molecules on the substrate
332 surface and the specific functional group(s) of the molecules bound to the substrate (Luo H,
333 Huang Y, Lai K, Rasco AB, Fan Y, 2016).

334 The SERS response of four different AuNPs colloids was compared with the aim to select the
335 best enhancing system for our scope. As demonstrated in Figure 3, all the AuNPs tested were
336 able to enhance the specific peaks of pyrimethanil in SERS analysis compared to the normal

337 Raman spectroscopy. The peak at 997 cm^{-1} was used to compare the intensity of the different
338 AuNPs because it exhibits the highest intensity and it is characteristic of the breathing mode
339 of the PMT aromatic ring (Herzberg G, 1988). The analytical enhancement factor (EF) for
340 each size of AuNPs was calculated using (2), where I_{SERS} and I_{NR} are the intensity of the
341 vibrational peak in SERS and normal Raman (NR) measurements, respectively, and C_{NR} and
342 C_{SERS} are the concentration of PMT in NR measurements and the SERS measurements,
343 respectively (Kara S et al. 2016):

$$EF = \frac{I_{\text{SERS}}C_{\text{NR}}}{1 + I_{\text{NR}}C_{\text{SERS}}} \quad (2)$$

344

345

Fig. 3

346 The EF increases together with AuNPs size, the highest value is reached when the 120 nm
347 AuNPs are used as reported in Table 1S in supplementary information. It is known that the
348 local electromagnetic enhancement increases with the increasing particle size (Kelly KL,
349 Coronado E, Zhao LL, Schatz GC, 2003) and as soon as the particles get bigger also the SP
350 band red-shifts, moving closer to the excitation wavelength of the laser (780 nm). This
351 probably explains our observations that the SERS EF generated from AuNPs is maximized
352 when the size of the gold NPs is around 120 nm. Moreover, we can infer that 120 nm AuNPs
353 arrange in a more suitable morphology in terms of roughness and vicinity of NPs on the
354 contaminated surface. Therefore, 120 nm AuNPs were selected and used for the further
355 development of the present methodology.

356 In order to demonstrate a practical application in the food safety field, green apples were
357 contaminated with PMT trace residues and *in situ* detection of the fungicide on a real sample
358 was initially tested. The surface of a green apple was contaminated by depositing 1 μl of PMT
359 concentrated suspension (40 μg of PMT) on the peel. 0.5 cm^2 area was covered approximately

360 in order to create an ultra-contaminated zone on the peel. Normal Raman mapping was
361 performed on the contaminated area but no or very low signals of PMT were collected on the
362 surface even if the local concentration is $80 \mu\text{g cm}^{-2}$ (Figure 4a). In order to increase the
363 sensitivity of the technique, a concentrated suspension of 120 nm AuNPs was spread as
364 “smart dust” over the contaminated area and SERS mapping was conducted. As Figure 4b
365 shows, the typical fingerprint of the PMT was registered after AuNPs deposition and its
366 spatial distribution on the surface was easily monitored by the micro-mapping Raman system.
367 A color scale bar from blue to red was associated to the intensity of the specific PMT peak at
368 997 cm^{-1} and related to the x,y position on the analyzed surface in order to provide a semi-
369 quantitative information of the PMT amount on the apple peel.

370 **Fig. 4**

371 Raman mapping presented in Figure 4 clearly demonstrated that *in situ* detection of PMT on
372 the apple peel only occurs when AuNPs are applied on the surface, while very low or no PMT
373 signals were registered in the contaminated regions without AuNPs. This means that normal
374 Raman technique is not sensitive enough to detect low amounts of PMT on the surface which
375 is further confirmed by an increase of the signal to noise ratio (S/N) from $S/N = 1.2$ for NR to
376 $S/N = 5$ for SERS measurements. Therefore, this approach could be easily used to achieve *in*
377 *situ* detection of PMT and to discriminate the type of fungicide/pesticide on the fruit surface
378 based on the specificity of the Raman fingerprint. However, this methodology would not be
379 reliable enough to provide a quantitative information on the entire surface of the apple due to
380 fact that only a small portion of the surface is analyzed and the colloids tend to randomly
381 aggregate on such inhomogeneous surfaces, such as fruits peel, leading to a lack of
382 reproducibility when spot-to-spot tests are conducted and when different fruit specimen are
383 compared.

384 In order to develop a quantitative methodology for PMT detection on the entire surface of the
385 fruit, a simple extraction procedure was first carried out to recover pyrimethanil from the
386 surface, as explained in the paragraph 2.7. An external calibration was chosen to set up the
387 analytical procedure. Five concentrations of pyrimethanil (0, 5, 10, 20, 40 mg kg⁻¹) were used
388 for the calibration curve and deposited by drop casting on a silicon dioxide surface. Silicon
389 dioxide was chosen as model substrate because its roughness does not contribute to the SERS
390 effect, its surface can be easily cleaned by any organic contamination and minimal
391 interference is provided by its Raman peaks. A concentrated suspension of 120 nm AuNPs
392 was deposited on each PMT spot and Raman mapping was applied to scan all the surface and
393 to overcome inhomogeneity problems. An average spectrum of each map was calculated and
394 normalized to the AuNPs peak at 2130 cm⁻¹, which was considered as internal reference to
395 eliminate the matrix effect, environmental parameters (temperature and humidity),
396 instrumental settings (focal distance) and to overcome variations of the enhancement effect
397 due to the different ratio between the amount of AuNPs and analyte molecules at each
398 standard concentration. SERS peaks at 997 cm⁻¹ of PMT standards on silicon dioxide are
399 shown in Figure 5a. To obtain the calibration curve, normalized SERS intensities at 997 cm⁻¹
400 were plotted as a function of PMT concentration. A WTLS regression was used for fitting the
401 data of PMT concentrations and Raman intensities taking into account their associated
402 variance. The uncertainty associated with the concentration values on x axis was calculated by
403 combining together, according to the law of uncertainty propagation, the different sources of
404 uncertainties which affect the solution concentration (B-type contributions due to the purity of
405 the PMT and the volume measurement). The obtained uncertainties are shown, for each point
406 in Figure 5b, as standard uncertainty bars (with coverage factor $k = 1$) parallel to the x axis.
407 The standard uncertainty associated with y values (reported as y error bars in Figure 5b) was

408 calculated as A-Type uncertainty on the basis of the standard deviation of the intensities at
409 997 cm^{-1} within each Raman map. A linear regression was found between the normalized
410 Raman signal at 997 cm^{-1} and the PMT concentration range between 0 - 40 mg kg^{-1} . The
411 forcefulness of the fit was confirmed by the reduced chi-square value (i.e. the sum of the
412 weighted squared residuals normalized by the number of degrees of freedom) which is
413 attested close to 1 in the considered concentration range. It is worthy to mention that the linear
414 correlation between concentration and SERS intensity is not held in wider concentration
415 range, because saturation effects of the SERS saturation effect are observed at higher
416 contaminant concentration. A drastic decreasing of the enhancement factor is registered for
417 more concentrated solutions. The LOD of the method, intended as three times the standard
418 deviation of the blank divided by the calibration curve slope is 4.74 ppm.

419

Fig. 5

420 However, even if the WTLS regression provided good linearity as demonstrated by low χ^2
421 value, the calculated uncertainty for slope and intercept are 14 % and 19 %, respectively.
422 These values are not negligible and they might affect the reliable quantification of PMT on
423 real samples. Therefore, it was decided to test a multivariate approach in order to minimize
424 the random variability associated to a single variable and to consider simultaneously the
425 whole information contained in spectral data. **A new calibration method was set up using PLS**
426 **regression to increase the method stability. The plot of the cumulative variance explained**
427 **(Figure 6a) and the RMSECV (Figure 6b) versus the number permit to determine a reasonable**
428 **number of component and to define a proper model complexity. For a number of LVs higher**
429 **than 8 no meaningful information is added, further LVs explain just experimental noise and**
430 **random variability. A “chemical-shape” is conserved in the loading until LV8 (Figure 3S),**
431 **then only random variability and experimental noise is carried by further LVs. Useful plots**
432 **for the model evaluation are reported in supplementary information (Figure 4S, 5S). The**
433 **method provides an RMSECV (root mean square error in cross validation) of 4.78 mg kg^{-1}**
434 **and cumulative explained variance of 87.06 %. The model was then validated with 4 samples**

435 contaminated with a nominal PMT concentration of 16 ppm providing an RMSEP of 4.03 mg
436 kg⁻¹. Both calibration and validation samples are shown in Figure 6c.

437

438

Fig. 6

439 In order to compare the performances of the two proposed methods, green apples spiked with
440 PMT at 7 mg kg⁻¹ were analyzed with both methods. The contaminant was recovered from the
441 apple peel following the optimized washing procedure described in section 2.7. A
442 contamination level of 8.65 ± 4.09 mg kg⁻¹ and 6.89 ± 3.06 mg kg⁻¹ as an average of 4
443 measurements was obtained using the calibration procedures based on WTLS and PLS,
444 respectively. Both values were in agreement with the spiked amount of PMT (7 mg kg⁻¹) on
445 the apple, demonstrating the reliability of both methodologies. However, the mean percentage
446 error (MPE) calculated over 5 repeated measurements was 32.8 % for the univariate
447 calibration and 18.7 % for the PLS. These results confirm that PLS methodology provides
448 higher accuracy and intra-day repeatability than univariate analysis and it is more suitable for
449 PMT detection on pome fruits.

450

451 4. Conclusions

452 A sensitive and rapid method to detect, discriminate and quantify residues of the fungicide
453 pyrimethanil on pome fruits was developed by means of AuNPs and Raman spectroscopy.
454 Spheroidal AuNPs with different size were fabricated and tested to determine the highest
455 enhancement factor (EF) for pyrimethanil detection. The analytical procedure was set up on a
456 silicon dioxide flat surface, here proposed as model system, to standardize SERS
457 methodology for both qualitative and quantitative analysis. A Raman mapping strategy was
458 exploited to increase signal reproducibility from spot to spot analysis and to minimize bias
459 due to different local surface morphologies, which historically affects SERS measurements.
460 The optimized methodology was tested on apples providing: i) a semi-quantitative *in situ*
461 detection of the fungicide on the contaminated fruit surface in case of highly contaminated

462 fruits; ii) a metrological tool for pyrimethanil quantification on the entire surface of pome
463 fruits in accordance with the European law limits. A validation set was used to define the
464 prediction capability of the model and, most of all, to demonstrate that the multivariate
465 approach is much worthy in case of a quantitative calibration of enhanced Raman spectra. In
466 fact, the overall spectral features are better captured and modeled in a multivariate approach
467 rather than in a univariate calibration, which just considers the Raman intensity at one single
468 wavelength, leaving out all other information contained in the spectrum. Even if the present
469 study does not cover the huge variability of natural samples and further studies are required to
470 prove its efficacy on fruits with different surface chemistry and morphology, the method here
471 developed guaranties sensitivity and repeatability levels compliant with the application needs
472 and paves the new way to the calibration of quantitative methods based on SERS for tracing
473 hazardous chemicals on non-wrinkled fruit surfaces.

474 **Acknowledgements**

475 The present work has been supported by EMRP project “ Q-AIMDS”. EMRP is jointly
476 founded by EMRP participating countries within EURAMET and the European Union.

477 Part of this work was carried out by NanoFacility Piemonte, INRiM, a laboratory supported
478 by Compagnia di San Paolo (Italy).

479

480 **References**

481 Amvrazi EG, Tsiropoulos NG (2009) Application of single-drop microextraction coupled
482 with gas chromatography for the determination of multiclass pesticides in vegetables with
483 nitrogen phosphorus and electron capture detection. Journal of Chromatography A 1216
484 (14):2789-2797.

485 **Becke AD (1993) Density-functional thermochemistry. III. The role of exact exchange.**
486 **Journal of Chemical Physics 98: 5648–5652.**

487 Commission Directive 2006/74/EC of 21 August 2006 amending Council Directive
488 91/414/EEC to include dichlorprop-P, metconazole, pyrimethanil and triclopyr as active
489 substances.

490 Evaluation of measurement data – Guide to the expression of uncertainty in measurement,
491 JCGM 100:2008 (GUM 1995 with minor corrections)

492 Evaluation of measurement data – Supplement 1 to the "Guide to the expression of
493 uncertainty in measurement" – Propagation of distributions using a Monte Carlo method,
494 JCGM101:2008,
495 http://www.bipm.org/utils/common/documents/jcgm/JCGM_101_2008_E.pdf. Accessed
496 [20/02/2017](http://www.bipm.org/utils/common/documents/jcgm/JCGM_101_2008_E.pdf)

497 FAO/ WHO, Pesticide Residues in Food 2007: Joint FAO-WHO Meeting on Pesticide
498 Residues”, <ftp://ftp.fao.org/docrep/fao/010/a1556e/a1556e00.pdf>, last accessed 19-06-2017

499 Fan Y, Lai K, Rasco BA, Huang Y (2014) Analyses of phosmet residues in apples with
500 surface-enhanced Raman spectroscopy. Food Control 37:153-157.

501 Frens, G. (1973). Controlled Nucleation for the Regulation of the Particle Size in
502 Monodisperse Gold Suspensions. Nature Physical Science 241:20-22.

503 Garrido JMPJ, Rahemi V, Borges F, Brett CMA, Garrido EMPJ (2016) Carbon nanotube
504 beta-cyclodextrin modified electrode as enhanced sensing platform for the determination of
505 fungicide pyrimethanil. Food Control 60:7-11.

506 **Gaussian 03, Revision B.05, References cited in <<http://www.gaussian.com>>.**

507 Gilden RC, Huffling K, Sattler B (2010) Pesticides and Health Risks. Jognn-Journal of
508 Obstetric Gynecologic and Neonatal Nursing 39 (1):103-110.

509 Gonzalez-Rodriguez RM, Rial-Otero R, Cancho-Grande B, Simal-Gandara J (2008)
510 Determination of 23 pesticide residues in leafy vegetables using gas chromatography-ion trap
511 mass spectrometry and analyte protectants. *Journal of Chromatography A* 1196:100-109.

512 He L, Chen T, Labuza TP (2014) Recovery and quantitative detection of thiabendazole on
513 apples using a surface swab capture method followed by surface-enhanced Raman
514 spectroscopy. *Food Chemistry* 148:42-46.

515 Herzberg G (1988) Citation Classic - Molecular-Spectra and Molecular-Structure .2. Infrared
516 and Raman-Spectra of Polyatomic-Molecules. *CC/Eng Tech Appl Scis* (13):16-16.

517 Hong S, Li X (2013) Optimal Size of Gold Nanoparticles for Surface-Enhanced Raman
518 Spectroscopy under Different Conditions. *Journal of Nanomaterials*
519 <http://dx.doi.org/10.1155/2013/790323>.

520 Kara SA, Keffous A, Giovannozzi AM, Rossi AM, Cara E, D'Ortenzi L, Sparnacci K,
521 Boarino L, Gabouze N and Soukane S (2016) Fabrication of flexible silicon nanowires by self
522 assembled metal assisted chemical etching for surface enhanced Raman spectroscopy. *RSC*
523 *Advances* 6: 93649–93659.

524 Kelly KL, Coronado E, Zhao LL, Schatz GC (2003) The optical properties of metal
525 nanoparticles: The influence of size, shape, and dielectric environment. *Journal of Physical*
526 *Chemistry B* 107 (3):668-677.

527 Lee C, Yang W, Parr RG (1998) Development of the Colle-Salvetti correlation-energy
528 formula into a functional of the electron density. *Physical Review B* 37: 785–789.

529 Li JF, Huang YF, Ding Y, Yang ZL, Li SB, Zhou XS, Fan FR, Zhang W, Zhou ZY, Wu DY,
530 Ren B, Wang ZL, Tian ZQ (2010) Shell-isolated nanoparticle-enhanced Raman spectroscopy.
531 *Nature* 464 (7287):392-395.

532 Li JF, Tian XD, Li SB, Anema JR, Yang ZL, Ding Y, Wu YF, Zeng YM, Chen QZ, Ren B,
533 Wang ZL, Tian ZQ (2013) Surface analysis using shell-isolated nanoparticle-enhanced
534 Raman spectroscopy. *Nature Protocols* 8 (1):52-65.

- 535 Liu B, Han G, Zhang Z, Liu R, Jiang C, Wang S, Han M-Y (2012) Shell Thickness-
536 Dependent Raman Enhancement for Rapid Identification and Detection of Pesticide Residues
537 at Fruit Peels. *Analytical Chemistry* 84 (1):255-261.
- 538 Luo H., Huang Y., Lai K. a, Rasco A. B., Fan Y. (2016) Surface-enhanced Raman
539 spectroscopy coupled with gold nanoparticles for rapid detection of phosmet and
540 thiabendazole residues in apples. *Food Control* 68:229-235.
- 541 Mercader JV, Esteve-Turrillas FA, Agullo C, Abad-Somovilla A, Abad-Fuentes A (2012)
542 Antibody generation and immunoassay development in diverse formats for pyrimethanil
543 specific and sensitive analysis. *Analyst* 137 (23):5672-5679.
- 544 Ortelli D, Edder P, Corvi C (2004) Multiresidue analysis of 74 pesticides in fruits and
545 vegetables by liquid chromatography-electrospray-tandem mass spectrometry. *Analytica*
546 *Chimica Acta* 520 (1-2):33-45.
- 547 Park S, Lee SJ, Kim HG, Jeong WY, Shim J-H, El-Aty AMA, Jeong SW, Lee WS, Kim ST,
548 Shin SC (2010) Residue analysis of multi-class pesticides in watermelon by LC-MS/MS.
549 *Journal of Separation Science* 33 (4-5):493-501.
- 550 Raepfel C, Nief M, Fabritius M, Racault L, Appenzeller BM, Millet M (2011) Simultaneous
551 analysis of pesticides from different chemical classes by using a derivatisation step and gas
552 chromatography-mass spectrometry. *Journal of Chromatography A* 1218 (44):8123-8129.
- 553 Review of the existing maximum residue levels (MRLs) for pyrimethanil according to Article
554 12 of Regulation (EC) No 396/2005, *EFSA Journal* 2011;9(11):2454
- 555 Rodriguez-Cabo T, Rodriguez I, Ramil M, Cela R (2011) Dispersive liquid-liquid
556 microextraction using non-chlorinated, lighter than water solvents for gas chromatography
557 mass spectrometry determination of fungicides in wine. *Journal of Chromatography A* 1218
558 (38):6603-6611.
- 559 Schluecker S (2014) Surface-Enhanced Raman Spectroscopy: Concepts and Chemical
560 Applications. *Angewandte Chemie-International Edition* 53 (19):4756-4795.

- 561 Sharma RR, Singh D, Singh R (2009) Biological control of postharvest diseases of fruits and
562 vegetables by microbial antagonists: A review. *Biological Control* 50 (3):205-221.
- 563 Socrates G “Infrared and Raman Characteristic Group Frequencies: Tables and Charts”,
564 Wiley ISBN: 978-0-470-09307-8.
- 565 Wold, H. (2006) Partial Least Squares. *Encyclopedia of Statistical Sciences*,
566 doi:10.1002/0471667196.ess1914.pub2
- 567 Yang J, Wang Q, Zhang M, Zhang S, Zhang L (2015) An electrochemical fungicide
568 pyrimethanil sensor based on carbon nanotubes/ionic-liquid construction modified electrode.
569 *Food Chemistry* 187:1-6.
- 570 Yu C, Zhou T, Sheng K, Zeng L, Ye C, Yu T, Zheng X (2013) Effect of pyrimethanil on
571 *Cryptococcus laurentii*, *Rhodosporidium paludigenum*, and *Rhodotorula glutinis* biocontrol of
572 *Penicillium expansum* infection in pear fruit. *International Journal of Food Microbiology* 164
573 (2-3):155-160.
- 574 Zheng J, He L (2014) Surface-Enhanced Raman Spectroscopy for the Chemical Analysis of
575 Food. *Comprehensive Reviews in Food Science and Food Safety* 13 (3):317-328.
- 576 Zhou Y, Han L, Cheng J, Guo F, Zhi X, Hu H, Chen G (2011) Dispersive liquid-liquid
577 microextraction based on the solidification of a floating organic droplet for simultaneous
578 analysis of diethofencarb and pyrimethanil in apple pulp and peel. *Analytical and*
579 *Bioanalytical Chemistry* 399 (5):1901-1906.
- 580 CCC software link, <https://www.inrim.eu/research-development/quality-life/ccc-software>
581 (last accessed 16-06-2017)
- 582 EC regulation No 396/2005, *EFSA Journal* 2011;9(11):2454

583

584 **FIGURE LEGENDS**

585 **Figure 1** - UV-Vis absorption spectra of AuNPs with the mean diameter of a) 30 nm, b) 55
586 nm, c) 90 nm and d) 120 nm (black curves); UV-Vis spectra of AuNPs stock suspension
587 mixed in a 2:1 ratio with pyrimethanil standard suspension 400 mg l⁻¹ at pH~3 (red curves);
588 repetition of UV-Vis measurements after four days (green curves).

589 **Figure 2** – Raman spectrum of pure Pyrimethanil with the characteristic vibrational peaks'
590 assignments.

591 **Figure 3** – a) Normal Raman spectrum of 400 mg l⁻¹ PMT on flat gold surface;
592 Representative SERS spectra of 400 mg l⁻¹ PMT using AuNPs with a mean diameter of b)
593 30 nm, c) 55 nm, d) 90 nm and e) 120 nm on a flat gold surface. Raman mapping of each
594 PMT-AuNPs spot was created by plotting the profile intensity of the PMT peak at 997 cm⁻¹
595 over the scanned area with a color scale bar from blue to red.

596 **Figure 4** – a) Normal Raman mapping of PMT contaminated region on fresh apple peel;
597 b) SERS mapping of PMT contaminated region on fresh apple peel after deposition of 120
598 nm AuNPs. The color scale bar for both a) and b) chemical images is related to the intensity
599 of the PMT peak at 997 cm⁻¹.

600 **Figure 5** – a) Normalized SERS spectra of 120 nm AuNPs with 5 levels of PMT standard in
601 negative matrix pool (representative of the analyzed matrix): 0, 5, 10, 20 and 40 mg kg⁻¹;
602 b) Calibration curves of PMT standards in negative matrix pool obtained by plotting the
603 normalized intensity of PMT Raman band at 997 cm⁻¹ vs. PMT concentration.

604 **Figure 6** – PLS calibration plots: a) Cumulative Explained Variance %; b) Root Mean Square
605 Error in Calibration and in Cross Validation versus the number of PLS latent variables; c) plot

606 of fitted value corresponding to calibration standards (grey) and validation samples (red)
607 versus the true values.

Figure1

[Click here to download high resolution image](#)

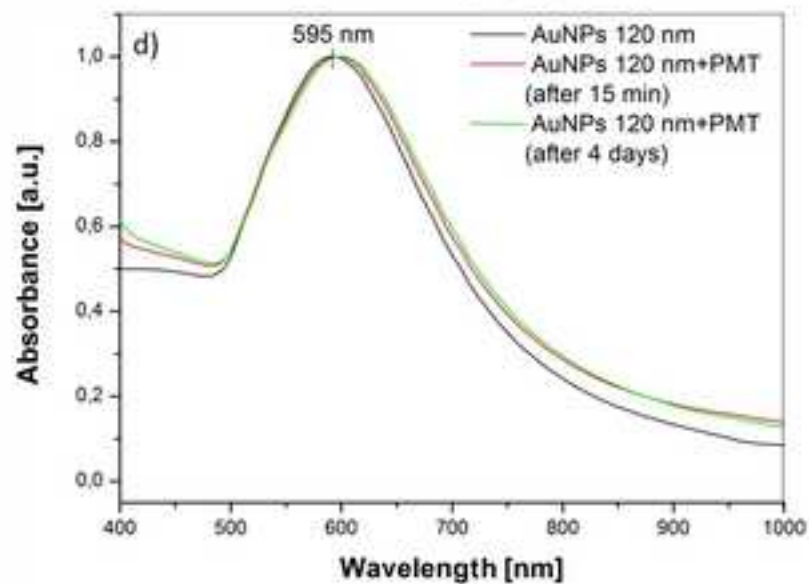
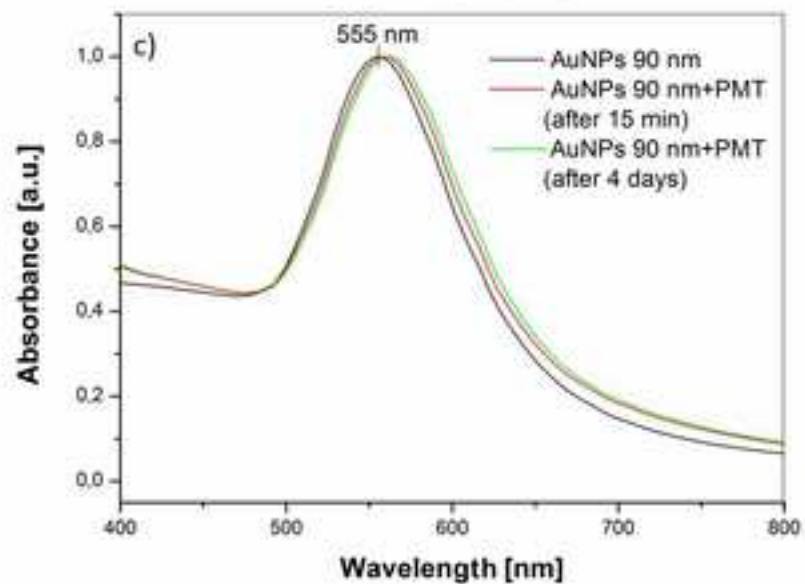
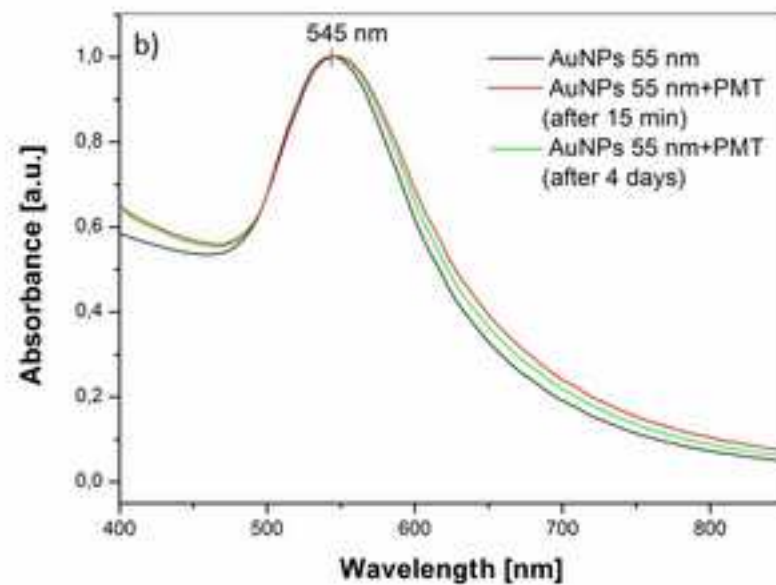
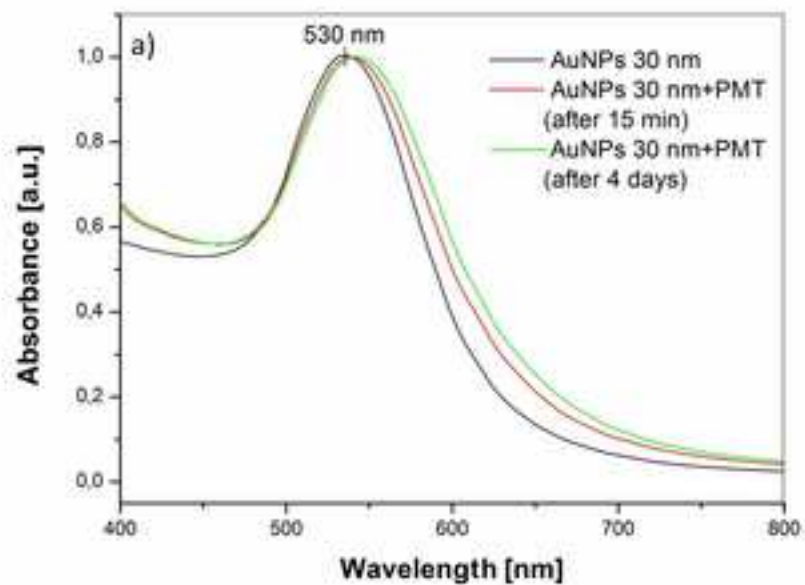


Figure 2

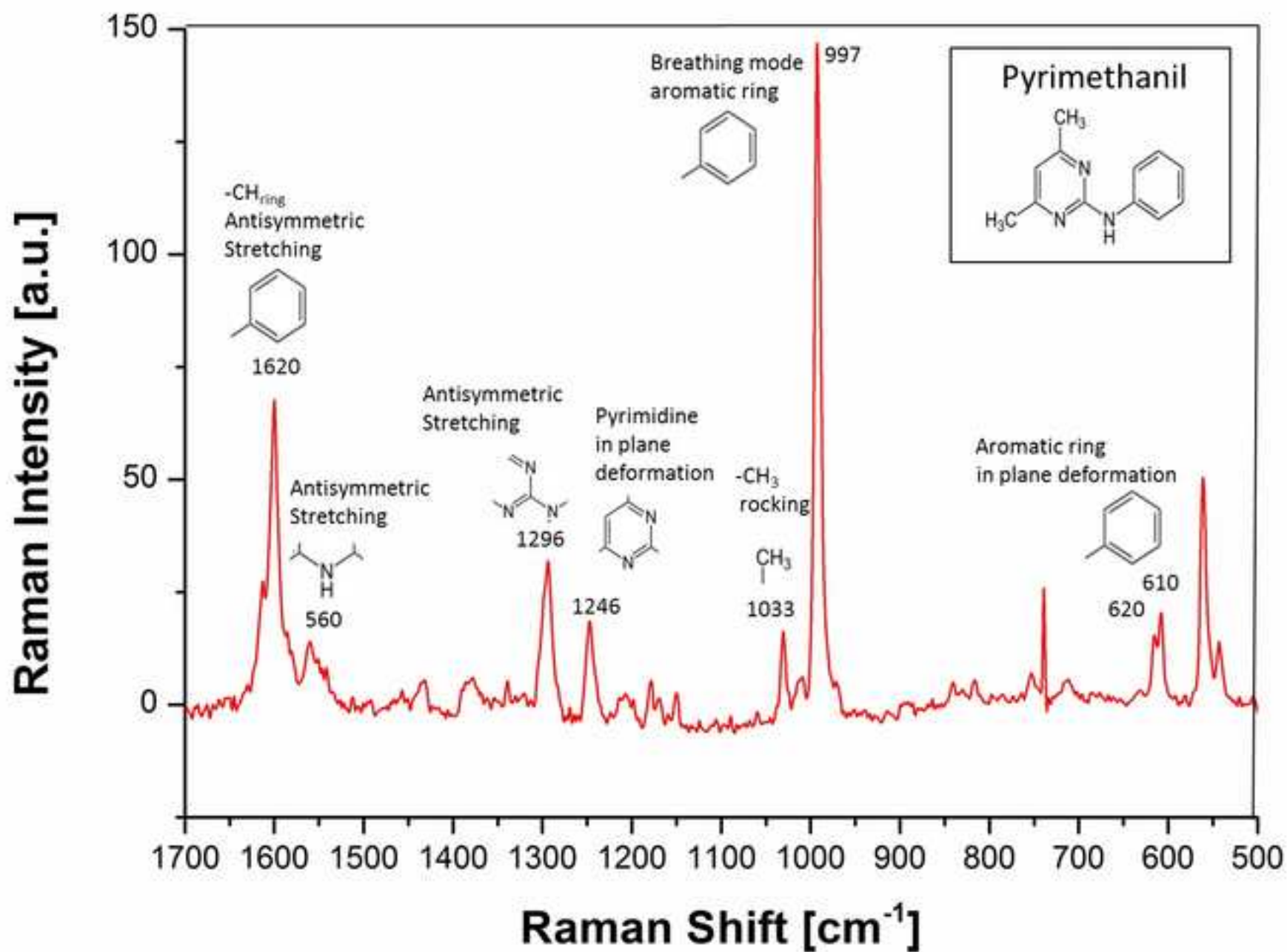
[Click here to download high resolution image](#)

Figure3
[Click here to download high resolution image](#)

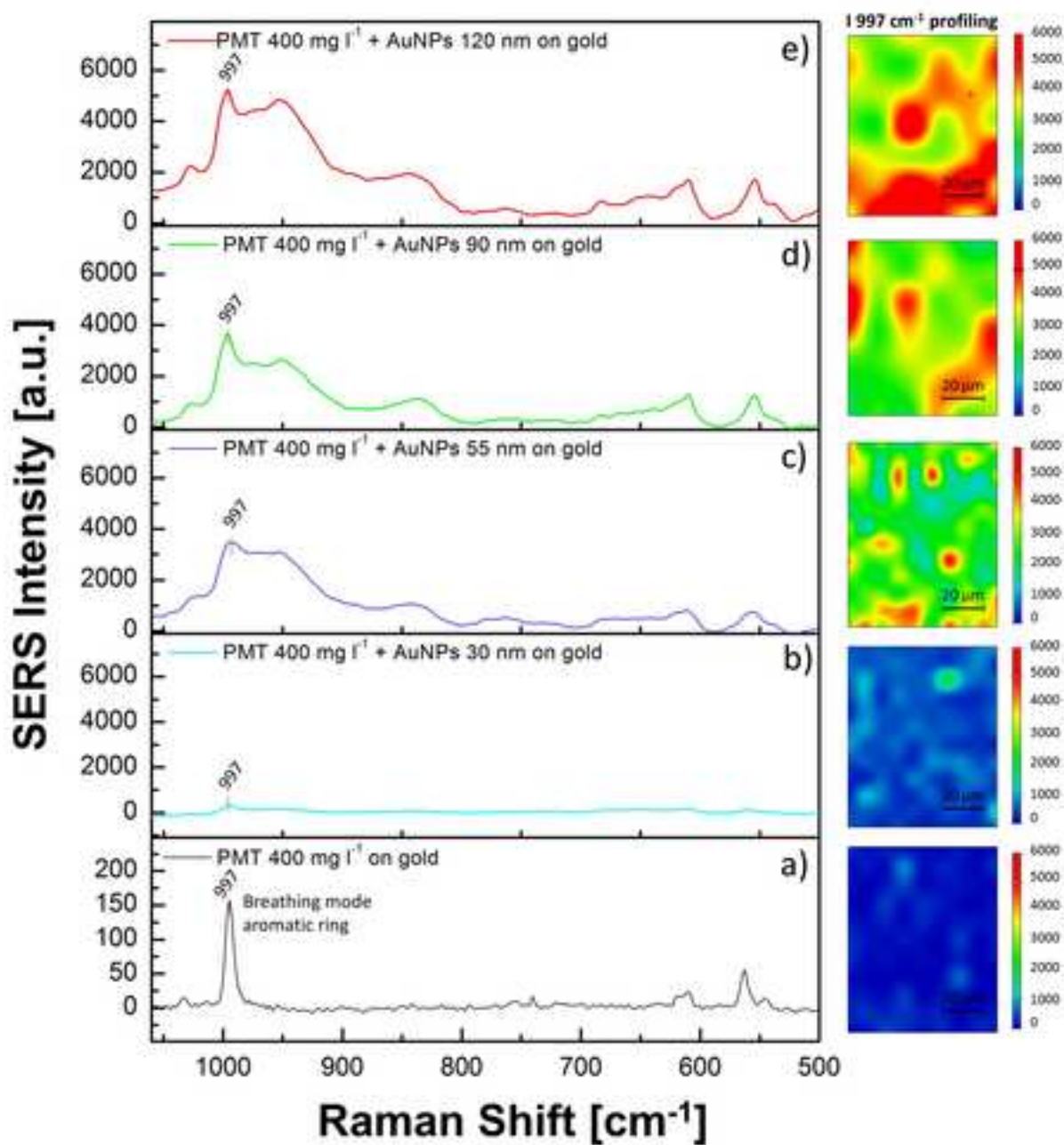


Figure4

[Click here to download high resolution image](#)

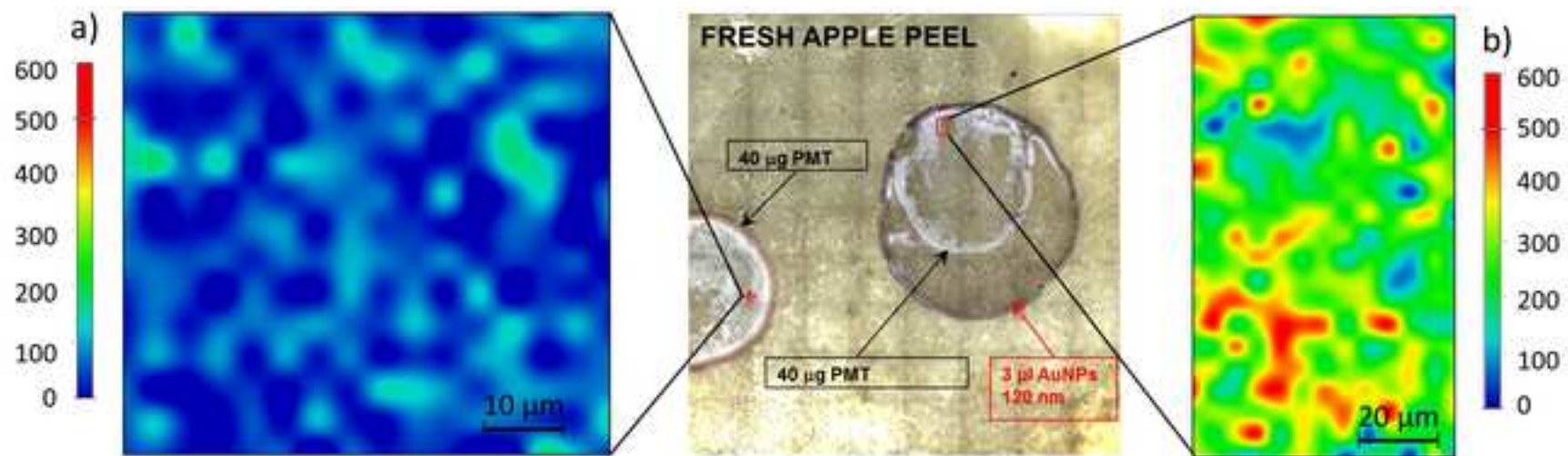


Figure5

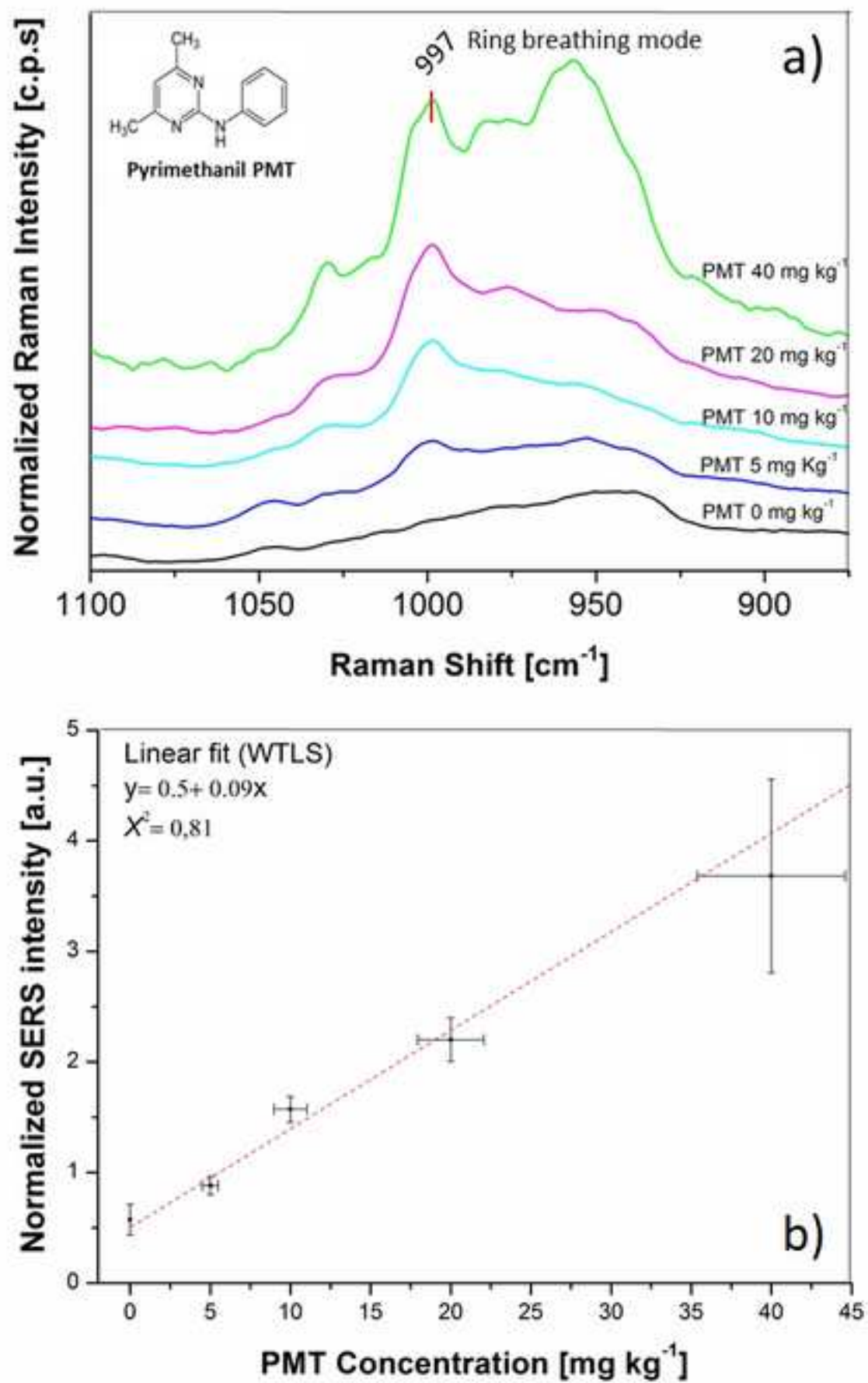
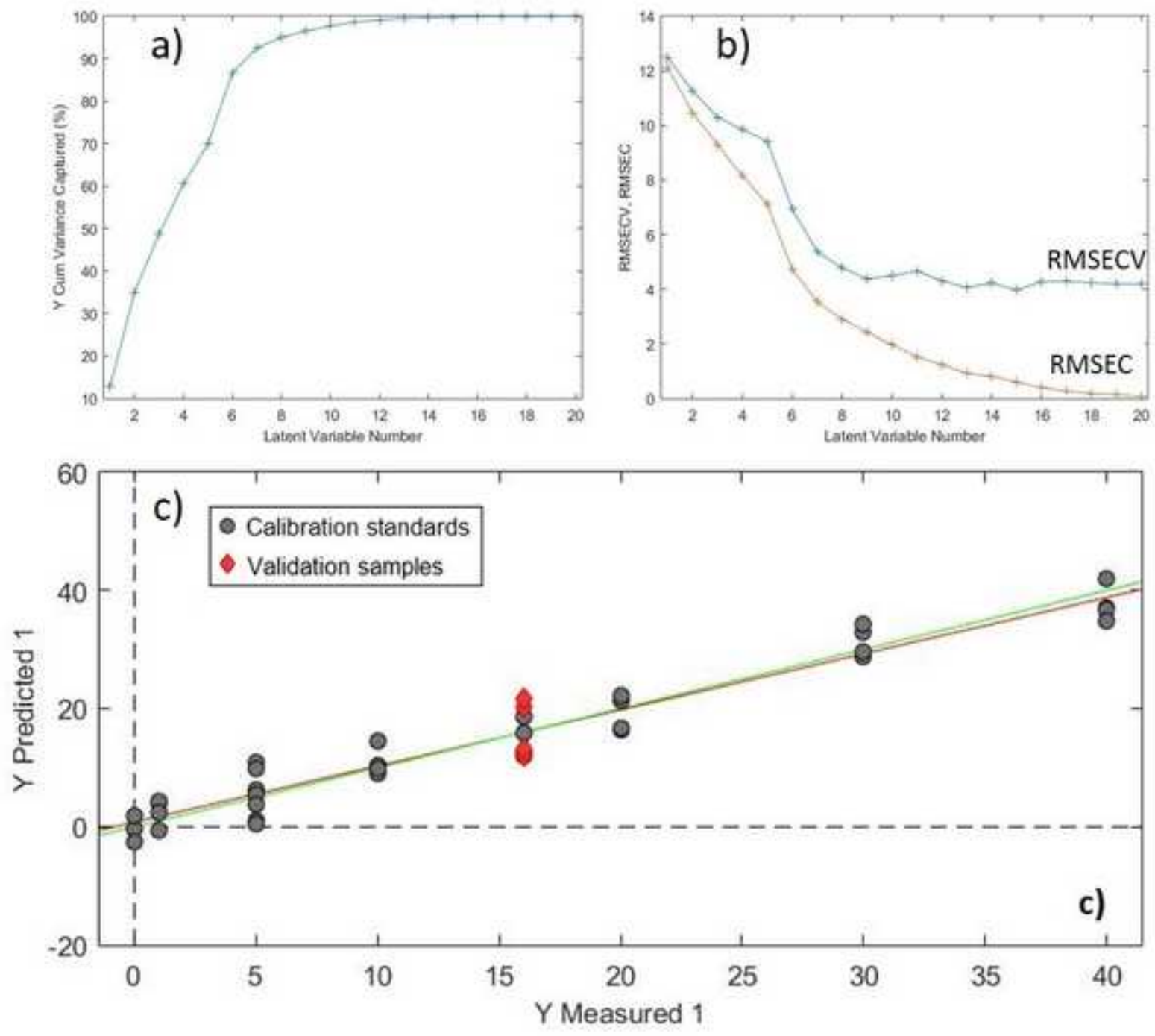
[Click here to download high resolution image](#)

Figure6

[Click here to download high resolution image](#)



Supplementary Material

[Click here to download Supplementary Material: Supplementary_Information_final.docx](#)

Highlights

- A rapid and sensitive method to detect pyrimethanil on apples is presented
- Raman signals of the pesticide are enhanced by drop casting AuNPs on the fruit peel
- 120 nm gold nanoparticles provide the best SERS response for this application
- Raman mapping strategy allows to overcome inhomogeneity problems
- Quantitative calibration using Partial Least Squares provides good method stability